Front. Phys. China, 2010, 5(2): 183–187
DOI 10.1007/s11467-010-0017-7

RESEARCH ARTICLE

Energy band and band-gap properties of deformed single-walled silicon nanotubes

Guang-cun SHAN (单光存)[1,2,†], Wei HUANG (黄维)[1]

[1] *Institute of Advanced Materials (IAM), Nanjing University of Posts and Telecommunications, Nanjing 210003, China*
[2] *Department of Materials Science, Fudan University, Shanghai 200433, China*
E-mail: 041055004@fudan.edu.cn

Received February 4, 2010; accepted March 12, 2010

The fantastic physical properties of single-walled silicon nanotubes (SWSiNTs) under mechanical strain make them promising materials for fabricating nanoscale electronic devices or transducers. Here we investigate the energy band and band-gap properties of the SWSiNTs calculated from the tight-binding model approximation. The results show that the band-gap properties are very sensitive to the deformation degree and the helicity of the SWSiNTs. The results can be employed to guide the design of nanoelectronic devices based on silicon nanotubes.

Keywords silicon nanotubes, band gap, deformed, energy band

PACS numbers 62.25.+g, 73.22.-f, 78.55.-m, 73.63.Fg

1 Introduction

Bottom-up assembly of nanoengineered materials holds promise for enabling a variety of applications in nanoelectronic devices with high integration density leading to enhanced performances [1–6]. Silicon nanotubes (SiNTs) are the most attractive because of the advantage of being compatible with today's integrated circuit technology for bulk silicon, as well as having controllable diameter and electronic properties during synthesis [4–8]. Except for the fascinating photoelectric and electronic properties like silicon nanowires [1–3], SiNTs also have great potential applications in energy conversion and storage owing to their considerable hollow cavities [5–15].

In the past few years, the synthesis of SiNTs has been demonstrated by various groups, each using a different growth process [5–8]. In 2002, Yang *et al.* [6, 7] first reported the synthesis by chemical vapor deposition and experimental observation by transmission electron microscopy (TEM) of large-diameter SiNTs (50 nm). Recently, Si nanotubes (SiNTs) have been investigated to elucidate the structural and electronic properties [11–14]. The results indicate that, under appropriate conditions, single-walled silicon nanotubes (SWSiNTs) may be stabilized. Fagan *et al.* [11] have investigated the structural and electronic properties of chiral SWSiNTs based on density functional theory (DFT) and claimed that Si hexagonal single-walled nanotubes may exhibit metallic or semiconductor behaviors, similar to the corresponding carbon nanotubes. Seifert *et al.* [12] have studied the mechanical and electronic properties of SWSiNTs using DFT tight-binding (TB) method and concluded that all these structures are semiconducting. Ponomarenko *et al.* [13] studied the energetics and their electronic structures compared with single-walled carbon nanotubes (SWCNTs). Using the first principles method, Yang *et al.* [4] found that the electronic properties of SWSiNTs have similar electronic properties with SWCNTs depending on different diameters and chiral vectors, and the large Si hexagonal single-walled nanotubes can be explained using the tight-binding model and the method of Brillouin zone foldings.

It is well known that the physical properties of the nanotubes depend much on their geometric structures, and so can be easily changed by an applied pressure or strain, which could be used to fabricate the nanoscale devices and transducers. Due to the experimental surroundings, the SWSiNTs may be subjected to various mechanical deformations. The effects of deformations, especially uniaxial tensile and torsional strains, on the energy bands and electronic properties of SWSiNTs are of great interest, offering the potential applications in nanoelectronic devices, and have attracted much attention. In this work, we present a simple picture of the strain effect on the energy band change of hexagonal SWSiNTs using the tight-binding model. The theoretical investigations showed that both uniaxial tensile and torsional

©Higher Education Press and Springer-Verlag Berlin Heidelberg 2010

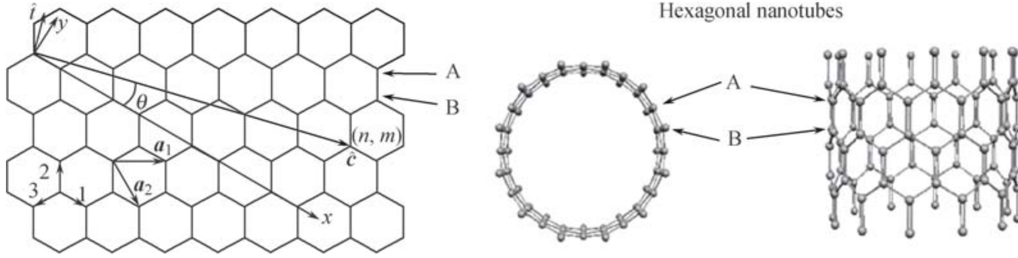

Fig. 1 Geometric structure of a silicon nanotube sheet. $\boldsymbol{r}_1$, $\boldsymbol{r}_2$, and $\boldsymbol{r}_3$ correspond to bond 1, 2, and 3, respectively. $\boldsymbol{a}_1$ and $\boldsymbol{a}_2$ are the lattice vectors of the two-dimensional sheet. $\hat{c}$ and $\hat{t}$ are unit vectors along the circumference and tube axis, respectively.

strains have a great impact on the energy band structures of the SWSiNTs.

2 Theory and Model

Hexagonal Si nanotubes (h-SiNTs) are formed by rolling the Si graphite-like sheet structure in analogy with CNTs, as shown in Fig. 1. When rolled into hexagonal SiNTs, two inequivalent atoms (A, B) have equal distance to the axis of the nanotubes. Similar to SWCNTs, A (n, m) SWSiNT can be viewed as a silicon graphite sheet rolled up into a cylinder and can be defined by two-dimensional lattice vector $\boldsymbol{R} = n\boldsymbol{a}_1 + m\boldsymbol{a}_2$, where $\boldsymbol{a}_1$ and $\boldsymbol{a}_2$ are primitive lattice vectors and m, n are a pair of integers. $C_h = a_0\sqrt{n^2+m^2+nm}$ is the circumference of a nanotube in the equilibrium lattice constant $|\boldsymbol{a}_1| = |\boldsymbol{a}_2| = a_0 (= 3.85$ Å). The bond vectors are given by

$$\boldsymbol{r}_1 = \frac{a_0}{2}\frac{n+m}{C_h/a_0}\hat{c} - \frac{a_0}{2\sqrt{3}}\frac{n-m}{C_h/a_0}\hat{t} + \delta\boldsymbol{r}_1 \tag{1-a}$$

$$\boldsymbol{r}_2 = -\frac{a_0}{2}\frac{m}{C_h/a_0}\hat{c} + \frac{a_0}{2\sqrt{3}}\frac{2n+m}{C_h/a_0}\hat{t} + \delta\boldsymbol{r}_2 \tag{1-b}$$

where $\delta\boldsymbol{r}_i$ represents deviation from an undeformed sheet and $\boldsymbol{r}_3 = -(\boldsymbol{r}_1 + \boldsymbol{r}_2)$. A cell in the nanotube can be labeled by a pair of integers (g, h), which is determined by a chiral vector $\boldsymbol{r} = g\boldsymbol{a}_1 + h\boldsymbol{a}_2$, as shown in Fig. 1. The electronic states of a nanotube allowed by the Born–von Kármán boundary condition $\boldsymbol{k}\cdot\boldsymbol{R} = 2\pi l$ lie on parallel lines perpendicular to $\boldsymbol{R}$. Furthermore, a deformed SWSiNT by uniaxial and torsional strains can be constructed when a 2-D strain tensor $\overleftrightarrow{\varepsilon} = (\varepsilon_{ij})_{2\times 2}$ is imposed. In the deformed nanotubes, real space vectors are $\boldsymbol{r} = (I+\varepsilon)\boldsymbol{r}_0$, where I is a unit matrix and $\boldsymbol{r}_0$ denotes the bond vector of the undeformed nanotubes. Within the context of continuum mechanics, application of a uniaxial or torsional strain causes the following change in the bond vectors of Fig. 1 [19]:

$$r_{it} \to (1+\varepsilon_t) r_{it} \quad \text{and} \quad r_{ic} \to (1+\varepsilon_c) r_{ic} \quad \text{(tensile)} \tag{2-a}$$

$$r_{ic} \to r_{ic} + \tan\gamma\, r_{it} \quad \text{(torsion)} \tag{2-b}$$

where, $i = 1, 2, 3$, and the superscripts t and c denote components along the tube axis and circumference. r_{ip} is the p component of $\boldsymbol{r}_i$. ε_t and ε_c represent the strains along the tube axis and circumference, respectively, in the case of uniaxial strain. The Poisson ratio v is equal to 0.2 (i.e., $\varepsilon_c = -0.2\varepsilon_t$) [16–18]. γ is the shear strain.

The lattice vectors of the deformed sheet are given by

$$\begin{aligned}\boldsymbol{a}_1 &= \boldsymbol{r}_1 - \boldsymbol{r}_3 \\ &= \frac{a_0}{2}\left[(1+\varepsilon_c)\frac{1}{2}\frac{2n+m}{C_h/a_0} + \tan\gamma\frac{\sqrt{3}}{2}\frac{m}{C_h/a_0}\right]\hat{c} \\ &\quad + a_0(1+\varepsilon_t)\frac{\sqrt{3}}{2}\frac{m}{C_h/a_0}\hat{t}\end{aligned} \tag{3}$$

$$\begin{aligned}\boldsymbol{a}_2 &= \boldsymbol{r}_1 - \boldsymbol{r}_2 \\ &= a_0\left[(1+\varepsilon_c)\frac{1}{2}\frac{n+2m}{C_h/a_0} - \tan\gamma\frac{\sqrt{3}}{2}\frac{n}{C_h/a_0}\right]\hat{c} \\ &\quad - a_0(1+\varepsilon_t)\frac{\sqrt{3}}{2}\frac{n}{C_h/a_0}\hat{t}\end{aligned} \tag{4}$$

The corresponding unit cell area is $|\boldsymbol{a}_1 \times \boldsymbol{a}_2| = \sqrt{3}/2(1+\varepsilon_t)(1+\varepsilon_c)a_0^2$.

As done in the study of the SWCNTs before [18, 19], the nanotube is treated within the approximation that it is a rolled up graphene sheet and assume a single-p orbital per silicon atom. Under the tight-binding (TB) approximation, the Hamiltonian of a (n, m) deformed nanotube is given by [16, 18]

$$H(\boldsymbol{k}) = \sum_{g,h,i} t_i \exp(\mathrm{i}\boldsymbol{k}\cdot\boldsymbol{r}_i) \tag{5}$$

where t_1, t_2, and t_3 represent the hopping parameters of the three kinds of deformed Si–Si bonds from a silicon atom with a bond length r_i and vector $\boldsymbol{r}_i = (I+\varepsilon)\boldsymbol{r}_{i0}$. The primary effect of the bond deformation is to alter the hopping parameters between the two nearest-neighbor atoms, which is assumed to be scale with the bond length relation $t_i = t_0(r_0/r_i)^2$ $(i = 1, 2, 3)$ [17–19].

Three t_i $(i = 1, 2, 3)$ are given as follows:

$$t_1 = t_0\frac{4\left(n^2+m^2+nm\right)}{\left[\sqrt{3}\,(n+m)\,(1+\varepsilon_c) - (n-m)\tan\gamma\right]^2 + \left[(n-m)\,(1+\varepsilon_t)\right]^2} \tag{6-a}$$

$$t_2 = t_0 \frac{4\left(n^2+m^2+nm\right)}{\left[-\sqrt{3}m\left(1+\varepsilon_c\right)+(2n+m)\tan\gamma\right]^2+\left[(2n+m)\left(1+\varepsilon_t\right)\right]^2} \tag{6-b}$$

$$t_3 = t_0 \frac{4\left(n^2+m^2+nm\right)}{\left[-\sqrt{3}n\left(1+\varepsilon_c\right)-(n+2m)\tan\gamma\right]^2+\left[(n+2m)\left(1+\varepsilon_t\right)\right]^2} \tag{6-c}$$

where the superscripts t and c denote components along the tube axis and circumference.

In this work, we take the parameters $a_0 = 0.385$ nm, $r_0 = 0.225$ nm, and $t_0 = 0.95$ eV, which are obtained by fitting the first principles calculations [4, 11]. Furthermore, diagonalization of the Hamiltonian gives the energy band structure of the (n, m) deformed nanotube sheet to be

$$\begin{aligned} E_{\pm}(k_t) = \pm \Bigg\{ & t_1^2+t_2^2+t_3^2+2t_1t_2\cos\left[\pi N\frac{n+2m}{n^2+nm+m^2}-\frac{\sqrt{3}}{2}\frac{n}{\sqrt{n^2+nm+m^2}}k_t\left(1+\varepsilon_t\right)a_0\right. \\ & \left.-\pi N\frac{\sqrt{3}\tan\gamma}{1+\varepsilon_c}\ \frac{n}{n^2+nm+m^2}\right]+2t_1t_3\cos\left[\pi N\frac{2n+m}{n^2+nm+m^2}+\frac{\sqrt{3}}{2}\frac{mk_t\left(1+\varepsilon_t\right)a_0}{\sqrt{n^2+nm+m^2}}\right. \\ & \left.+\pi N\frac{\sqrt{3}\tan\gamma}{1+\varepsilon_c}\ \frac{m}{n^2+nm+m^2}\right]+2t_2t_3\cos\left[\pi N\frac{n-m}{n^2+nm+m^2}\right. \\ & \left.\left.+\frac{\sqrt{3}}{2}\frac{(n+m)k_t\left(1+\varepsilon_t\right)a_0}{\sqrt{n^2+nm+m^2}}+\pi N\frac{\sqrt{3}\tan\gamma}{1+\varepsilon_c}\ \frac{n+m}{n^2+nm+m^2}\right]\right\}^{1/2} \end{aligned} \tag{7}$$

where $N = 0, 1, \ldots, N_{c-1}$ (N_c is the hexagon number in a unit cell), and $-\pi/T \leqslant k \leqslant \pi/T$ with T, the deformed 1-D lattice constant determined by $T = (1+\varepsilon_t)\sqrt{3}C_h/\gcd(2n+m, 2m+n)$. Here, gcd refers to the largest common divisor. The plus and minus subscripts above stand for the conduction and valence bands, respectively. The energy band of a (n, m) nanotube in the presence of uniaxial ($\gamma = 0$) or torsional strain ($\varepsilon_t = \varepsilon_c = 0$) can be calculated from Eqs. (1)–(7).

3 Results and discussion

Based on TB calculations, now we present our theoretical analysis of $(n, 0)$ zigzag and (n, n) armchair SWSiNTs for different n values for zigzag and armchair structures.

We first consider the case of uniaxial strain. The band gap is obtained by finding the minimum of $E(k_t)$, where the values of k_t and N are spanned and analyzed. Figures 2 and 3 show the energy bands for the (10, 10) and (10, 0) nanotubes under tensile strain with $\varepsilon_t = 3\%$ and $\varepsilon_t = 6\%$. As shown in Fig. 2 and Fig. 4, for armchair tubes, the uniaxial strain does not cause change in band gap; but for zigzag tubes, the magnitude of the band-gap change is approximately equal to $3t_0$, which is similar to the results of the corresponding SWCNTs [16, 18, 19]. Besides, as shown in Fig. 4, it is found that under uniaxial strain, the derivative of band gap over strain is the largest for zigzag tubes and decreases with increase of the chiral angle.

As uniaxial strain increases, there is an abrupt reversal in sign of the magnitude of the band-gap change $|E_g/\mathrm{d}\sigma|$ as illustrated for zigzag tubes in Fig. 4. This feature indicates a change in band index N corresponding to the band gap and can be understood from the following expression that describes dependence of energy band struc-

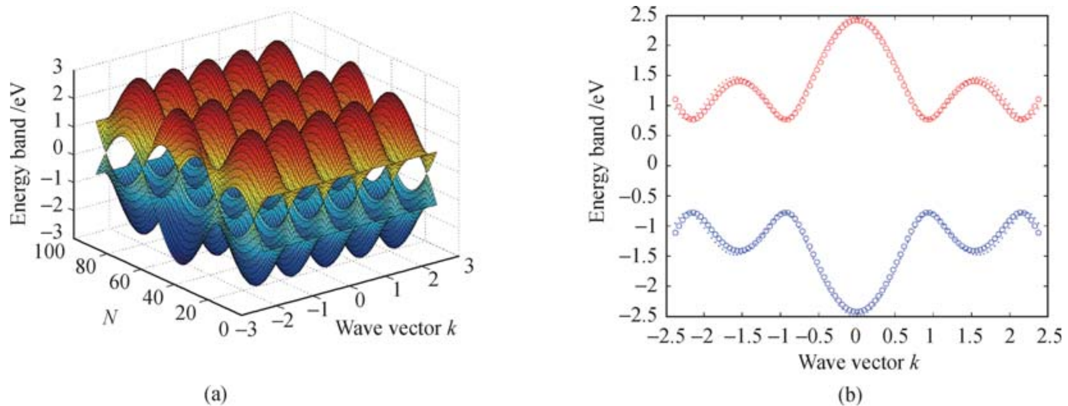

Fig. 2 **(a)** Energy band for the (10, 10) tube under tensile strain $\varepsilon_t = 3\%$. **(b)** Change of $N = 3$ energy band for the (10, 10) tube under tensile strain. The dotted and circle line correspond to 3% and 6% strains, respectively. Here, k is in unit of $1/a_0$.

ture of $(n, 0)$ nanotubes for various values of N:

$$E(k_t) = \pm t_2 \left\{ 1 \pm \frac{4t_1}{t_2} \cos \frac{N\pi}{n} \cos \left[(1+\varepsilon_t) \frac{\sqrt{3}}{2} k_t a_0 \right] + \left(\frac{2t_1}{t_2} \right)^2 \cos^2 \frac{N\pi}{n} \right\}^{1/2} \quad (8)$$

The minimum of $E(k_t)$ occurs at $k_t = 0$, given by

$$E(0) = \pm t_2 \left| 1 - \frac{2t_1}{t_2} \cos \frac{N\pi}{n} \right| = E_0(N) - 2t_0 \frac{\delta r_1}{r_0} \left(1 - 2\frac{\delta r_2}{\delta r_1} \cos \frac{N\pi}{n} \right) \left(1 - 2\cos \frac{N\pi}{n} \right) \quad (9)$$

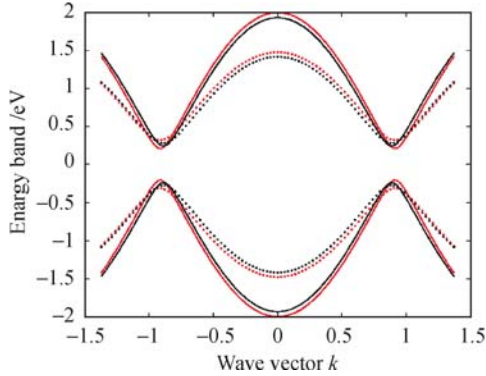

Fig. 3 Change of $N = 3$ (*solid line*), and $N = 4$ (*dotted line*) energy bands for the (10, 0) tube under tensile strain. The red and black lines correspond to 3% and 6% strains, respectively. Here, k is in unit of $1/a_0$.

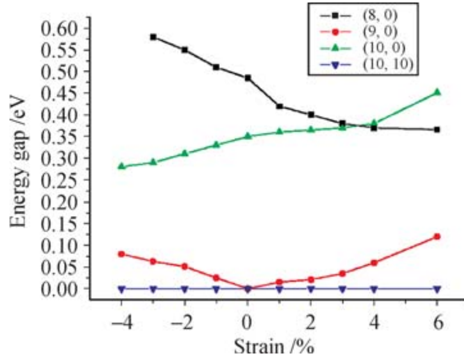

Fig. 4 Band gap versus tensile strain.

The minimum value of $E_0(N) = t_0|1 - 2\cos(N\pi/n)|$ is half of the band gap of an unstrained nanotube. The first term of Eq. (9) takes the smallest value for the band index $N = N_0$ that satisfies $n = 3N_0 + 1$. However, the second term can change sign when N changes from N_0 to $N_0 + 1$. As a result, a dramatic change in sign of $\mathrm{d}E_\mathrm{g}/\mathrm{d}\sigma$ becomes possible if the magnitude of the second term is larger than the change in the first term. For the (10, 0) tube, the change in slope occurs at around nine percent strain. These strain values are accessible in bulk nanotube samples. Figure 3 shows the change in the $N = 3$ and $N = 4$ energy bands for the (10, 0) tube for different values of tensile strain. While the $N = 3$ band shifts up in energy as strain increases, the $N = 4$ band shifts down, which leads to the corresponding change in sign of $\mathrm{d}E_\mathrm{g}/\mathrm{d}\sigma$.

In case of torsional strain, the band gap is obtained by finding the minimum of $E(k_t)$ using Eq. (7). Figure 5 shows the $N = 3$ energy bands for the (10, 0) nanotubes under torsional strain with $\gamma = 1°$ and $\gamma = 2°$. As shown in Fig. 5 and Fig. 6, for the $(n, 0)$ zigzag tubes, the torsion strain doesn't cause too much change and only a slightly small band-gap change. For armchair tubes, the magnitude of the band-gap change $|E_\mathrm{g}/\mathrm{d}\sigma|$ is approximately equal to $3t_0$ independent of the diameter.

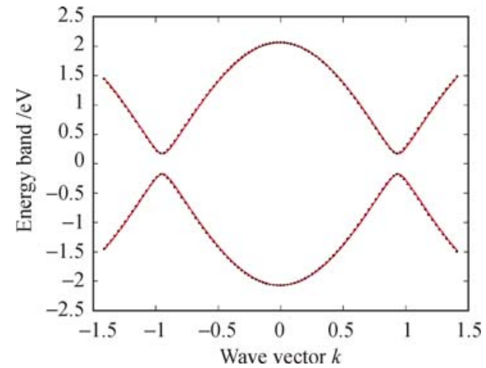

Fig. 5 Change of $N = 3$ energy bands for the (10, 0) tube under torsional strain. The red solid and black dotted lines correspond to 1° and 2° strains, respectively. Here, k is in unit of $1/a_0$.

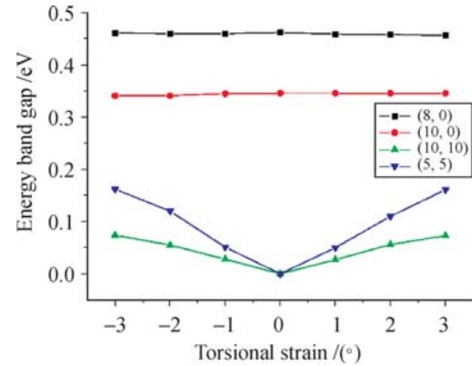

Fig. 6 Band gap versus torsional strain.

As a result of the hexagonal structural characteristic, some aspects of SWSiNTs exhibit similar oscillations as the SWCNTs, such as the energy gap of $(n, 0)$ nanotube with increasing n, and the energy gap of nanotube with increasing strains [17–19]. Mechanical strain red or blue shifts the energy levels of the SWSiNT depending on the types of strains induced and the value of $(n - m)$ mod 3 rule. Besides, most of the deformed SWSiNTs show a metal-semiconductor transition, occurring periodically with increasing strain. These oscillations can be understood in terms of periodic match between the Fermi wave vector $\boldsymbol{k}_\mathrm{F}$ and the lattice constant or the π bonding characteristics. Symmetry breaking due to the deformation

may remove the energy level degeneracy.

4 Conclusions

In conclusion, we present a simple picture to calculate energy band and band gap versus strain of SWSiNT. In the TB approximation, we have shown that the energy band and band-gap of single-walled silicon nanotube is sensitive to the uniaxial and torsional deformations. We find that some aspects of SWSiNTs exhibit similar oscillations as the SWCNTs, such as the energy gap of $(n,\ 0)$ nanotube with increasing n, and the energy gap of nanotube with increasing strains, due to the hexagonal structural characteristic. The results indicate that, under uniaxial strain, $|\mathrm{d}E_{\mathrm{g}}/\mathrm{d}\sigma|$ of zigzag tubes is $3t_0$ independent of diameter, and it takes the value zero for the armchair tubes. In contrast, under torsional strain, $|\mathrm{d}E_{\mathrm{g}}/\mathrm{d}\sigma|$ of armchair tubes is $3t_0$. The *ab initio* calculations on the effect of deformations on the band-gap change of SWSiNTs are in progress for further study and comparison. These results can be used in future applications of nanoelectronic devices based on SWSiNTs.

Acknowledgements This work was supported by the National Natural Science Foundation of China (Grant No. 60721004) and the National Basic Research Program of China (Grant No. 2009CB010600).

References

1. Y. Huang, X. F. Duan, Y. Cui, L. J. Lauhon, K. H. Kim, and C. M. Lieber, Science, 2001, 294: 1313
2. Y. Cui and C. M. Lieber, Science, 2001, 291: 851
3. Y. Cui, Q. Q. Wei, H. K. Park, and C. M. Lieber, Science, 2001, 293: 1289
4. X. Yang and J. Ni, Phys. Rev. B, 2005, 72: 195426
5. J. Bai, X. C. Zeng, H. Tanaka, and J. Y. Zeng, Proc. Natl. Acad. Sci. USA, 2004, 101: 2664
6. S. Y. Jeong, J. Y. Kim, D. Yang, B. N. Yoon, S. H. Choi, H. K. Kang, C. W. Yang, and Y. H. Lee, Adv. Mater., 2003, 15: 1172
7. J. Sha, J. Niu, X. Ma, J. Xu, X. Zhang, Q. Yang, and D. Yang, Adv. Mater., 2002, 14:1219
8. J. Hu, Y. Bando, Z. Liu, J. Zhan, and D. Golberg, Adv. Funct. Mater., 2004, 14: 610
9. G. C. Shan, M. Zhang, and W. Huang, Proceedings of 3rd IEEE International NanoElectronics Conference 2010 (INEC2010), 2010, 3: 181
10. A. S. Barnard and S. P. Russo, J. Phys. Chem. B, 2003, 107: 7577
11. S. B. Fagan, R. Mota, R. J. Baierle, G. Paiva, A. J. R. da Silva, and A. Fazzio, J. Mol. Struct. Theochem., 2000, 539: 101
12. G. Seifert, Th. Kohler, K. H. Urbassek, E. Hernandez, and Th. Frauenheim, Phys. Rev. B, 2001, 63: 193409
13. O. Ponomarenko, M. W. Radny, and P. V. Smith, Surface Science, 2004, 562: 257
14. M. Zhang, Y. H. Kan, Q. J. Zang, Z. M. Su, and R. S. Wang, Chem. Phys. Lett., 2003, 379: 81
15. M. De Crescenzi, P. Castrucci, M. Scarcelli, M. Diociauti, P. S. Chaudhari, C. Balasubramanian, T. M. Bhave, and S. V. Bhoraskar, Appl. Phys. Lett., 2005, 86: 231901
16. X. P. Yang, G. Wu, and J. M. Dong, Front. Phys. China, 2009, 4(3): 280
17. W. A. Harrison, Electronic Structure and the Properties of Solids, New York: Dover, 1989
18. L. Yang and J. Han, Phys. Rev. Lett., 2000, 85: 154
19. H. Jiang, Y. Zhang, G. Yu, and J. Dong, Phys. Lett. A, 2006, 351: 308